20

Infrared Spectroscopy Techniques in the Characterization of SOFC Functional Ceramics

Daniel A. Macedo et al.*
Material Science and Engineering Post Graduate Program, UFRN
Brazil

1. Introduction

Infrared spectroscopy is certainly one of the most important analytical techniques available nowadays for scientists. One of the greatest advantages of infrared spectroscopy is that virtually any sample in any physical state can be analyzed. The technique is based on the vibrations of atoms of a molecule. An infrared spectrum is obtained by passing infrared radiation through a sample and determining what fraction of the incident radiation is absorbed at a particular energy. The energy at which any peak in an absorption spectrum appears corresponds to the frequency of a vibration of a part of a sample molecule (Stuart, 2004).

Fourier transform infrared spectroscopy (FTIR) has been widely used for *in situ* analysis of adsorbed species and surface reactions. Infrared spectroscopy techniques have being used for the characterization of solid oxide fuel cells (SOFCs). FTIR is utilized to identify the structure of the SOFC electrode and electrolyte surface (Resini et al., 2009; Guo et al., 2010). Liu and co-workers (Liu et al., 2002) were pioneers in the *in situ* surface characterization by FTIR under SOFC operating conditions.

The development of high-performance electrode and electrolyte materials for SOFC is an important step towards reducing the fuel cell operation temperature to the low and intermediate range (500 – 700 ^{o}C). As the operating temperature is reduced, many cell parts, such as the auxiliary components can be easily and cost-efficiently produced. To meet long operational lifetime, material compatibility and thermomechanical resistance would be less critical as the range of possibilities for lower temperature increases. To that end, recent research at UFRN, Natal, Brazil has successfully focused on novel synthesis processes based on microwave-assisted combustion and modified polymeric precursor methods in order to synthesize high performance cobaltite-based composite cathodes for low-intermediary-temperature SOFCs.

* Moisés R. Cesário[2], Graziele L. Souza[3], Beatriz Cela[4], Carlos A. Paskocimas[1], Antonio E. Martinelli[1], Dulce M. A. Melo[1,2] and Rubens M. Nascimento[1]
[1]*Material Science and Engineering Post Graduate Program, UFRN, Brazil*
[2]*Chemistry Pos Graduate Program, UFRN, Brazil*
[3]*Chemical Engineering Department, UFRN, Brazil*
[4]*Forschungszentrum Jülich GmbH, Central Department of Technology (ZAT), Germany*

This book chapter reviews how powerful infrared spectroscopy techniques play a fundamental role in the novel synthesis approaches developed during the last 5 years (2007 – 2011) by this research group. Synthesized high performance cathode powders had their features investigated using different materials characterization techniques, such as Fourier Transform Infrared Spectroscopy (FTIR), FAR and MID-Infrared spectroscopy.

2. Solid oxide fuel cells and its components

Fuel cells are highly efficient power generation devices which convert chemical energy of gaseous fuels (hydrogen, fossil fuels and ethanol among others) directly into electric power in a silent and environmentally friendly way. These electrochemical devices are promising alternatives to traditional mobile and stationary power sources, such as internal combustion engines and coal burning power plants. Among the various types of fuel cells, solid oxide fuel cells (SOFCs) have advantages linked to high energy conversion efficiency and excellent fuel flexibility because of their high operating temperature compared to other types of fuel cells. Fig. 1 depicts a typical SOFC single cell produced by our research group. It consists of three basic components: two porous electrodes (anode and cathode) and a solid electrolyte. Each one of these components must fulfil specific performance requirements such as microstructural stability during preparation and operation; chemical and physical compatibility, i.e., similar thermal expansion coefficients; adequate porosity and catalytic activity to achieve the highest performance (Minh & Takahashi, 1995; Singhal, 2000).

The SOFC electrolyte material, typically yttria stabilized zirconia (YSZ) or rare earth doped ceria, must be an electronic insulating but ion-conducting ceramic that allows only protons or oxygen ions to pass through. Furthermore, the electrolyte material must be dense to separate the air and fuel, chemically and structurally stable over a wide range of partial pressures of oxygen and temperatures. The cathode (air electrode) material, typically lanthanum manganites and cobaltites, has to be electrocatalyst for oxygen reduction into oxide ions. When an oxygen ionic conducting oxide is adopted as electrolyte, these ions diffuse through the material to the anode (fuel electrode), driven by the differences in oxygen chemical potential between fuel and air constituents of the cell, where they electrochemically oxidize fuels such as hydrogen, methane, and hydrocarbons. The released electrons flow through an external circuit to the cathode to complete the circuit. The complete mechanism of electric power production in a SOFC is also shown in Fig. 1.

SOFCs have attracted significant attention in the last 20-30 years due to their high efficiency, fuel flexibility and environmental advantages (Minh, 2004; Molenda et al., 2007; McIntosh & Gorte, 2004). However, typical SOFCs operate at 1000 ºC. Elevated operating temperatures introduce a series of difficulties such as sintering of the electrodes and high reactivity between cell components. For these reasons, there is a considerable research interest in reducing the operating temperature of these devices down to the range between 500 and 800 °C, which characterizes intermediate temperature solid oxide fuel cells (IT-SOFCs) or even lower, which would imply the use of inexpensive metallic materials, rapid start-up and shut-down, minimization of thermal degradation and reactions between cell components, and longer operational lifetime. Furthermore, as the operation temperature is reduced, system reliability increases, increasing the possibility of using SOFCs for a wide variety of applications, including residential and automotive devices. On the other hand, reduced operating temperatures reduces the overall electrochemical performance due to increased

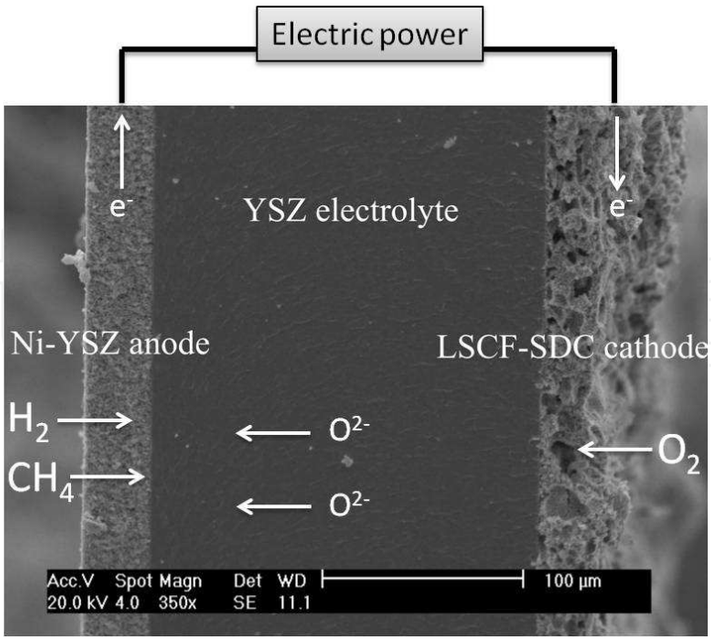

Fig. 1. A typical SOFC single cell with its basic components (anode, cathode and electrolyte) and the mechanism of energy production.

ohmic losses and electrode polarization losses associated with thermally activated processes of both ionic transport and electrode reactions. In special, the electrochemical activity of the cathode dramatically deteriorates with decreasing temperature for typical strontium-doped lanthanum manganite (LSM) based electrodes (Singhal 2000; Steele, 2000; Steele & Heinzel, 2001).

Thus, to achieve acceptable performance of IT-SOFCs, reducing the electrolyte resistance and electrode polarization losses are two key points. Losses attributed to electrolytes can be minimized by decreasing the thickness of electrolyte layers or substituting traditional YSZ by other electrolytes, such as doped ceria and apatite-like materials. The overall electrochemical limitation would then be ruled by electrode polarization losses. Due to the higher activation energy and lower reaction kinetics for oxygen reduction at the cathode compared with those of the fuel oxidation at the anode, the polarization loss from the air electrode (cathode) that limits the overall cell performance (Ivers-Tiffee et al., 2001; Tsai & Barnett, 1997). Therefore, the development of new cathode materials with high electrocatalytic activity for oxygen reduction becomes a critical issue for the development of IT-SOFCs.

2.1 Development of cathode materials

The development of high performance cathodes is based on reducing its thickness from hundreds to few micrometers associated with the addition of an electrolyte material in the formation of composite cathodes. These are interesting approaches that can improve electrode performance for the reduction of oxygen. The latter allows the extension of the triple phase boundaries (TPB) from the electrolyte/cathode interface deep into the bulk of the electrode, permitting electrochemical reactions to take place within the electrode. The

preparation of composite cathodes by the combination of strontium-doped lanthanum manganite (LSM) with yttria stabilized zirconia (YSZ) or even samarium oxide-doped ceria (SDC) has been intensively studied in the last years. Whereas rare earth doped ceria, both samarium (SDC) and gadolinium doped ceria (CGO), have higher ionic conductivity than YSZ. Thus, composite cathodes such as LSM-SDC or LSM-CGO have better electrochemical performance than LSM-YSZ, and are particularly indicated for IT-SOFCs (Zhang et al., 2007; Chen et al., 2008; Wang et al., 2007).

2.1.1 Lanthanum manganite and cobaltite based cathodes

Lanthanum manganites ($LaMnO_3$), particularly strontium-doped lanthanum manganites ($La_{1-x}Sr_xMnO_3$ - LSM), are widely used as cathode materials in SOFCs operating at high temperatures (800 – 1000 °C), which is the temperature range where yttria-stabilized zirconia (YSZ) is commonly used as electrolyte. Doping Sr into $LaMnO_3$ considerably increases electrical conductivity because of the increased number of holes. LSM cathodes present high stability, electro-catalytic activity for O_2 reduction at high temperatures and thermal expansion coefficient reasonably similar to YSZ electrolyte (Escobedo et al., 2008; Jiang, 2003; Minh, 1993). Even thought LSM cathodes have been successfully used as functional materials in high temperature SOFCs, they have been replaced for more efficient lanthanum strontium cobaltite ferrites (LSCF). LSMs are poor ionic conductors and the electrochemical reactions are limited to the region close to triple phase boundaries (TPB). On the other hand, LSCF is a mixed electronic/ionic conductor (MEIC) with appreciable ionic conductivity. The exchange of oxygen ions occurs at the electrode surface with the diffusion of oxygen through the mixed conductor (Liu et al., 2007; Shao et al., 2009).

Due to low ionic conductivity and high activation energy to oxygen dissociation at low temperatures, cathodes made of LSM and LSCF are normally combined with the electrolyte material forming a composite cathode. The composite cathodes containing ceria are more attractive to low and intermediate temperatures (500 – 700 °C) than the ones containing YSZ, which has lower ionic conductivity in such temperatures (Yang et al., 2007; Xu et al., 2006; Xu et al., 2005; Chen et al., 2007; Zhang et al., 2008; Lin et al., 2008).

Among the extensive number of chemical synthesis routes available for the preparation of LSM and LSCF powders, the polymeric precursor method (Pechini method), solid state reaction, spray pyrolysis and combustion synthesis have been successful used (Conceição et al., 2009; Cela et al., 2009; Grossin & Noudem, 2004; Guo et al., 2006; Macedo et al., 2009; Conceição et al., 2011). In spite of the proved efficiency of the polymeric precursor method to produce monophasic nanometric powders, alternative synthesis methods mainly using microwave technology have being implemented in an attempt to minimize energy consumption and total powder production time (Liu et al., 2007). An alternative method for preparing nanoparticles with particle sizes of order of nanometers using low annealing temperatures has been developed using commercial gelatin as a polymerizing agent. This method has been named by the authors as *soft chemical route* (Medeiros et al., 2004; Maia et al., 2006).

Regarding the development of LSM based composite cathodes, several works have reported the preparation of LSM-SDC cathodes from the powders obtained by different synthesis methods (Ye et al., 2007; Chen et al., 2007; Xu et al., 2009). However, no reports on the

preparation of LSM-SDC films from powders synthesized using commercial gelatin have been encountered. This chapter presents recent results in obtaining cathodes based on LSM and SDC powders obtained by the modified Pechini method using commercial gelatin as polymerizing agent. LSM-SDC films were prepared using different amounts of ethyl cellulose as pore former. Among the many methods which can be used to produce SOFC cathodes, slurry spin coating was selected due to its fast processing time and high uniformity over the surface. In this technique, a high spin rotation quickly lays the slurry on the substrate which dries in short times, hindering particle agglomeration, which also contributes to the uniform distribution of particles along the green film. The characteristics of not only LSM, SDC and LSCF powders, but also LSM-SDC spin-coated and LSCF-SDC screen-printed films have been investigated by different techniques.

3. Infrared spectroscopy techniques applied in the SOFC research

The fundamental studies of the catalytic reactions mechanisms that occur near the three-phase boundary in the anode of a solid oxide fuel cell still deserving attention and investigation. Many in situ spectroscopies such as Raman and infrared spectroscopy are routinely used in catalysis research to characterize surface intermediates and reaction mechanisms. It is very difficult to apply in situ spectroscopy techniques to an operating SOFC anode (Atkinson et al., 2004). Recently research groups (Liu et al., 2002; Guo et al., 2010) presented their methodologies on the possible ways to apply the infrared emission spectroscopy to characterize working SOFC anodes.

Guo and co-workers (Guo et al., 2010) worked recently developing a novel experimental technique to measure in situ surface deformation and temperature on the anode surface of a SOFC button cell, along with cell electrochemical performance under operating conditions. An adaptation of a SOFC button cell test apparatus was integrated with a Sagnac interferometric optical setup and IR thermometer. This optical technique was capable of in situ, noncontact, electrode surface deformation, and temperature measurement under SOFC operating conditions. The surface deformation measurement sensitivity is half-wavelength and is immune to temperature fluctuation and environmental vibration. The experimental data can be used for the validation and further development of SOFC structural and electrochemical modeling analyses (Guo et al., 2010).

Other application of infrared spectroscopy techniques, for example FTIR, is for functional ceramic, electrodes and electrolyte, characterization. Through analyze of the absorption bands in low wave number region the oxygen-metal linkage are associated; the enlarged bands are attributed to the stretching vibration of hydrogen-bonded OH groups present. Moreover, the residual carbon from the synthesis not eliminated in the thermal treatment processes, can also be observed in some bands, for example associated to carboxylate anion (COO-) stretching and the C-O groups or to stretching vibration of the C-O bonds.

4. Experimental

4.1 Preparation and characterization of functional materials for SOFC

During the last years the research of the group on SOFC development has been focused on the synthesis of $LaSrMnO_3$ (LSM), $SmCeO_2$ (SDC) and $LaSrCoFeO_3$ (LSCF) powders by two different methods. LSM and SDC powders have been prepared by the modified Pechini

method using gelatin as a polymerizing agent. LSCF powder has been synthesized by microwave-assisted combustion. The electrochemical performance of a single electrolyte-supported SOFC containing LSCF-SDC composite cathode film has also been investigated.

The raw materials used to synthesize LSM and SDC powders by the modified Pechini method, in which gelatin replaces ethylene glycol, were lanthanum, strontium, manganese (VETEC, Brazil), samarium and cerium (Sigma-Aldrich, Germany) nitrates. For synthesizing LSM, a solution of manganese citrate was firstly prepared from manganese nitrate and citric acid with a molar ratio of 1:3 (metal/citric acid) under stirring for 2 h at 70 °C. Stoichiometric amounts of the other citrates were added one by one at 1 hour intervals. The temperature was slowly increased up to 80 ^{o}C and then gelatin was added at a weight ratio of 40:60 (gelatin/citric acid). The solution was stirred on a hot plate, which allowed the temperature to be controlled until a polymeric resin was formed. This resin was pre-calcined at 300 °C for 2 h, forming a black solid mass which was grounded into a powder and calcined at 500, 700 or 900 °C for 4 h to obtain the LSM perovskite structure. SDC powder was obtained following the same procedure but calcined between 700 and 900 ^{o}C.

To further understand the synthesis mechanism used in this work, which uses gelatin instead of ethylene glycol, it is necessary to review the traditional polymeric precursor method proposed by Pechini (Pechini, 1967). The Pechini method involves the formation of stable metal-chelate complexes with certain alpha-hydroxycarboxyl acids, such as citric acid, and polyesterification in the presence of a polyhydroxy alcohol, such as ethylene glycol, to form a polymeric resin. The metal cations are homogeneously distributed in the polymeric resin, which is then calcined to yield the desired oxides. The most common materials used as source of cations are nitrate salts since they can be fully removed at low temperatures (400 – 500 ^{o}C). The synthesis mechanism of the modified Pechini method used in this work can be explained in three basic steps, as shown in Fig. 2. It stands out by its simplicity and low cost, using only citric acid, gelatin and metal nitrates as reagents.

In the first step, a solution of metallic citrate is prepared from the mixture of deionized water, citric acid and the salts of each metal ion. The citric acid acts as a chelating agent to remove metal ions from the solution. Chelation is the ability that a chemical substance has to form a ring-like structure with a metal ion, resulting in a compound with different chemical properties compared to the original metal, which prevents it from following different chemical routes. The chelating agent acts as a crayfish which traps the metal in its claws. When metal ions are in solution, they are surrounded by water molecules which avoid the establishment of new bonds. Thus, the chelating agent replaces such water molecules (bonds) and forms a ring-like structure, resulting in the phenomenon known as chelation. The number of binding sites that can form coordination bonds in the metal determines the number of rings formed.

The second step of this synthesis mechanism is the gelatin hydrolysis. Gelatin is a natural polymer, composed of a mixture of high molecular weight polypeptides (proteins) obtained by controlled hydrolysis of collagen fiber. Therefore, it can be used for cheap aqueous polymeric precursor synthesis in order to attain nanocrystalline powders. As illustrated in Fig. 2, the gelatin hydrolysis corresponds to the breaking of peptide bonds in the presence of water. For easier understanding, the second step reaction, in this illustration, is taking place in a low molecular weight peptide. An extra hydrogen ion is necessary to react with the -NH_2 group on the left-hand end of the peptide, the one not involved in the peptide bond. By

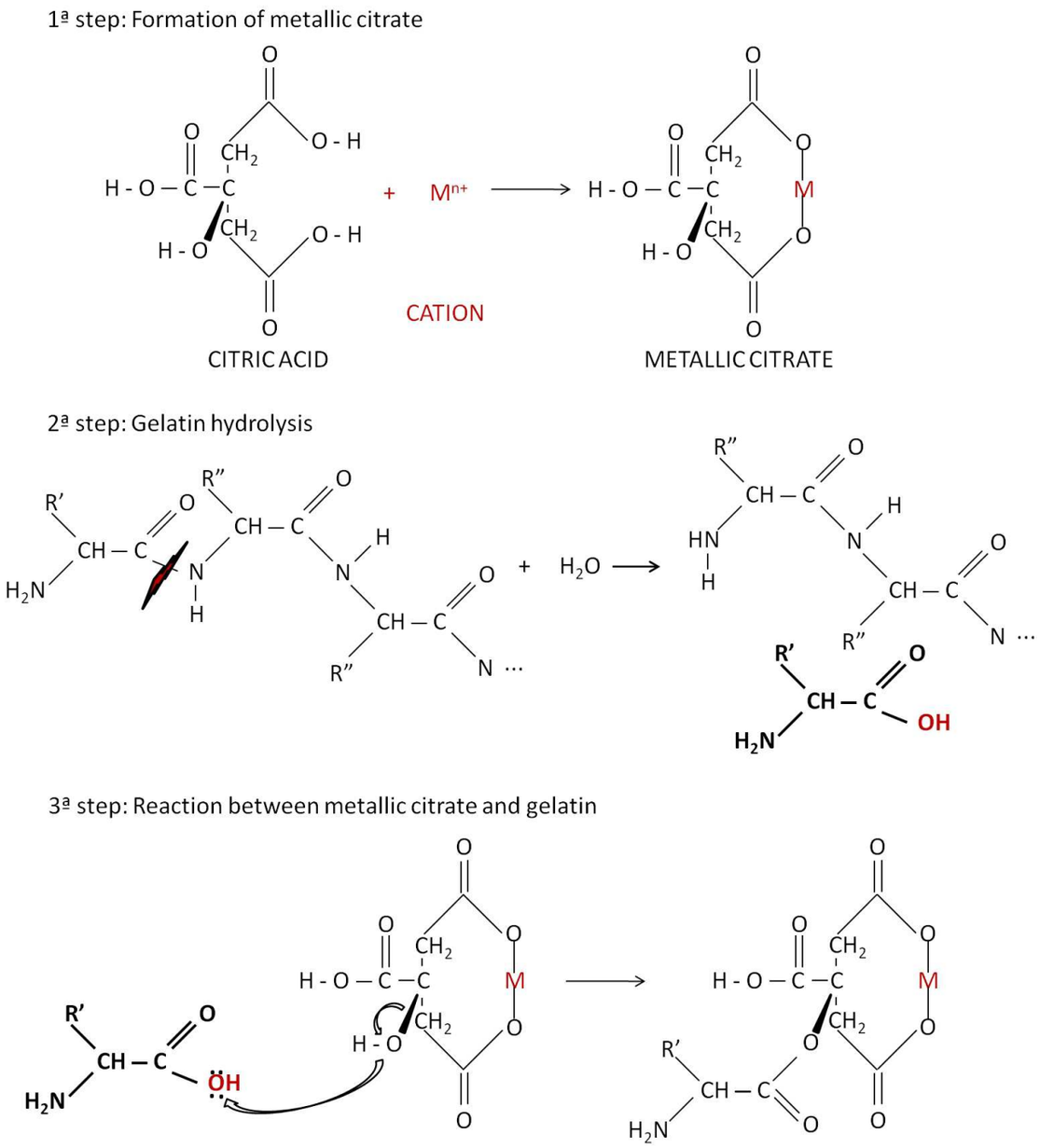

Fig. 2. Synthesis mechanism of the modified Pechini method.

scaling this up to a polypeptide (a protein chain), each of the peptide bonds will be broken in exactly the same way. This means that a mixture of the amino acids that makes up the protein will form, although in the form of their positive ions because of the presence of hydrogen ions from the citric acid. The presence of positive ions (not shown in Fig.2) is due to the fact that an amino acid has both a basic amine group and an acidic carboxylic acid group. There is an internal transference of a hydrogen ion from the -COOH group to the -NH_2 group to grant both a negative and positive charge to the ion. This is called a zwitterion. This is how amino acids exist even in the solid state. After being dissolved in water, the gelatin forms a simple solution which also contains this ion. A zwitterion is a compound with no overall electrical

charge, but which contains separate parts, positively and negatively charged. As the pH decreases by adding an acid to a solution of an amino acid, the -COO- side of the zwitterion picks up a hydrogen ion, forming the desirable compound.

In the third step, proteins act as amides and react with the free hydroxyl of the citric acid. The hydroxyl of the citric acid reacts like the hydroxyl of an alcohol in a standard esterification process. During the reaction of the amide with the citric acid, the substitution of the amide hydroxyl by an alkoxy radical (-OR) takes place. At the end of the process, the oxygen in the –OH group of the citric acid remains in the chain whereas the hydroxyl oxygen in the amino acids is eliminated in the form of water. This mechanism results in long chains containing metal cations tightly bond and evenly distributed.

To synthesize LSCF powders, an aqueous solution of $La(NO_3)_3$, $Sr(NO_3)_2$, $Co(NO_3)_2$, and $Fe(NO_3)_3$ (VETEC, Brazil) and urea as fuel was heated up to 100 ^oC under stirring for 10 minutes. Afterwards, the becker was placed in a microwave oven set to 810 W and 2.45 GHz. Self-ignition takes place in about 1 minute. The resulting powder was then calcined at 900 ^oC for 4 h in order to remove carbon residues remaining in the ash and to convert the powder to the desired LSCF phase with a well-defined crystalline perovskite structure.

LSM, SDC and LSCF powders were characterized by XRD using a Shimadzu XDR-7000 diffractometer and scanning electron microscopy (SEM-SSX 550, Shimadzu). Infrared spectra were also recorded with FTIR (IR Prestige-21, Shimadzu) in the 400 – 4600 cm^{-1} spectral range. Specific surface area measurements were performed only for the LSM powders. An infrared reflectance spectrum of a LSM pellet prepared from a powder calcined at 900 °C was recorded with a Fourier-transform spectrometer (Bomem DA 8-02) equipped with a fixed-angle specular reflectance accessory (external incidence angle of 11.5°).

4.1.1 Preparation and characterization of composite cathodes

Composite powders consisted of 50 wt.% cathode (LSM or LSCF) and 50 wt.% SDC were prepared by mixing in a ball mill for 24 h in order to deposit LSM-SDC and LSCF-SDC composite films by spin coating (LSM-SDC) and screen printing (LSCF-SDC). Prior to spin coating deposition, ceramic suspensions of LSM-SDC composite powders were prepared using ethanol and different amounts of ethyl cellulose as pore-forming material. Ethyl cellulose was added in the weight ratios of 4, 8 and 10 wt.% with respect to the total solid weight. With the purpose of studying the influence of the milling process on the particle size distribution, another mixture was prepared without milling and without the addition of ethyl cellulose. Before coating, the ceramic suspensions were ultrasonically treated and then deposited by spin coating onto YSZ substrates. Commercially available YSZ powder (Tosoh Corporation, Japan) was compressed into pellets (13 mm in diameter) under uniaxial pressure (74 MPa) and then sintered in air at 1450 °C for 4 h to increase its mechanical strength for application as ceramic substrate. In the deposition process, 25 layers were applied using initial and final rotation speeds of 500 rpm for 15 seconds and 5000 rpm for 30 seconds, respectively. The composite films were attained after sintering at 1150 °C for 4 h. LSCF-SDC cathodes were screen-printed onto YSZ electrolytes and sintered at 950 °C for 4 h. The morphological characterization of the surface and cross section of LSM-SDC composite cathodes was performed using a field emission gun scanning electron microscope (FEG-SEM, Zeiss-Supra 35) and a scanning electron microscope (SEM-SSX 550, Shimadzu).

4.2 Preparation and characterization of a SOFC single cell

A preliminary performance test was carried out to qualitatively evaluate the prepared LSCF-SDC composite cathode. A single SOFC supported on commercial, 200μm thick, YSZ electrolyte (Kerafol, Germany) with Ni-YSZ anode and LSCF-SDC composite cathode screen printed was used. To assemble the single cell, first the anode suspension was printed and the half cell was sintered at 1300 °C for 4 h. The anode was reduced during cell operation. Later on, the LSCF-SDC cathode was printed on the other electrolyte side and sintered at 950°C for 4 h to avoid undesirable reactions. An in-house test station was used in the performance evaluation. The single cell was tested using dry hydrogen as fuel and oxygen as oxidant, in the ratio of 40ml/min H_2 and 40ml/min O_2. The current–voltage characteristic of the cell was measured using linear sweep voltammetry (LSV) over a temperature range of 800 to 950 °C. The microstructure of the cathode/electrolyte interface after the performance test was examined by SEM.

5. Results and discussion

5.1 Characterization of functional materials for SOFC

XRD patterns of the calcined LSM powders can be observed in Fig. 3. The as-synthesized material depicts the main diffraction peaks characteristic of the rhombohedral structure with space group $R\bar{3}c$ (Konysheva et al., 2009) and the respective JCPDS (Joint Committee on Powder Diffraction Standards) chart number 53-0058. Secondary phases were found and identified as $SrCO_3$ and Mn_3O_4. The presence of $SrCO_3$ was identified at 500 and 700 ^oC by comparison with JCPDS pattern number 84-1778. The formation of strontium carbonate is due to the reaction between SrO and CO_2 produced during organic compound decomposition. Mn_3O_4 is present only in the powder calcined at 900 °C and was identified by comparison with pattern JCPDS 89-4837. It probably came from the change of oxidation state of the Mn ion. Vargas and co-workers (Vargas et al., 2008) have reported that

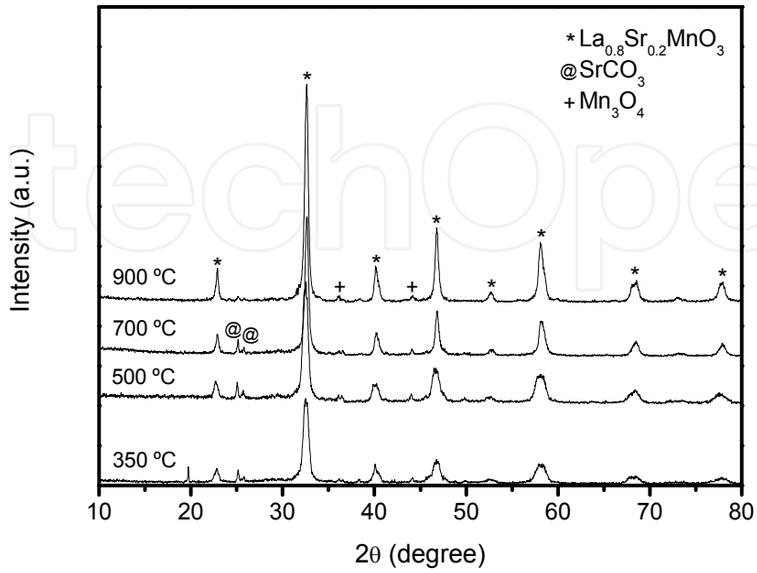

Fig. 3. XRD patterns of LSM powders calcined at different temperatures.

temperatures higher than 1000 °C are necessary to remove all the carbon present in the LSM powders. Lower calcination temperatures result in free carbon or as carbonates from the degradation of citrates.

Table 1 lists the specific surface area (S_{BET}), average crystallite size (D_{XRD}), average particle size (d_{BET}), microstrain and the d_{BET}/D_{XRD} ratio for LSM powders calcined at 700 and 900 °C. There is a clear dependency between the average crystallite size and the calcination temperature. The thermal treatment temperature is directly proportional to the crystallite size, because of the crystallization process that occurs in high temperatures. Therefore, the specific surface area decreases with the onset of particle sintering. High particle sizes promote lower surface area to volume ratio, which results in small deformations in the crystalline structure parameters.

Calcination temperature (°C)	S_{BET} (m^2/g)	d_{BET} (nm)*	D_{XRD} (nm)**	Microstrain (%)	d_{BET}/D_{XRD}
700	18.79	48.9	22.80	0.004869	2.1
900	8.46	108.7	25.21	0.003917	4.3

*Calculated from specific surface area
*Theoretical density: LSM= 6.521 g/cm^3
**Calculated by Rietveld refinement

Table 1. Specific surface area (S_{BET}), average particle size (d_{BET}), average crystallite size (D_{XRD}), microstrain and crystalline degree of LSM powders.

The d_{BET}/D_{XRD} ratio, which indicates the degree of particle agglomeration, increases with the calcination temperature. In a previous study (Cela et al., 2009), d_{BET}/D_{XRD} equal to 12 was established for the LSM powder synthesized with ethylene glycol as the polymerizing agent and calcined at 900 °C. This result shows that the substitution of ethylene glycol for gelatin reduces powder agglomeration, improving the potential to prepare ceramic suspensions to be deposited as cathode films with good adherence to the substrate.

LSM powders were observed by scanning electron microscopy (Fig. 4). SEM micrographs revealed the presence of soft particles agglomerates. Fig. 4(d) displays a FEG-SEM high magnification image of the LSM powder calcined at 900 °C. As it can be seen, this powder reveals strong agglomeration of particles with an estimated size lower than 100 nm. Results from SEM analyses are in good agreement with specific surface area measurements.

In the FTIR spectra of the LSM powders calcined between 500 and 900 °C, displayed in Fig. 5, a band located at 603 cm^{-1} is attributed to M – O (metal – oxygen) stretching, and is characteristic of the perovskite structure. On the other hand, bands corresponding to carbon bonds, particularly carboxyl groups are visible in 1000 – 2500 cm^{-1} interval. The two absorption bands at 1460 cm^{-1} and 2360 cm^{-1} are due to C=O vibration and can be related to traces of carbonate. In the range of 3300 – 3670 cm^{-1} a band corresponding to O – H bond can be attributed to adsorbed water due to the contact of the sample with the environment. With this information and the XRD analyses, it became clear that the carbonate content of the synthesized powders decreases and even vanishes at higher calcination temperatures.

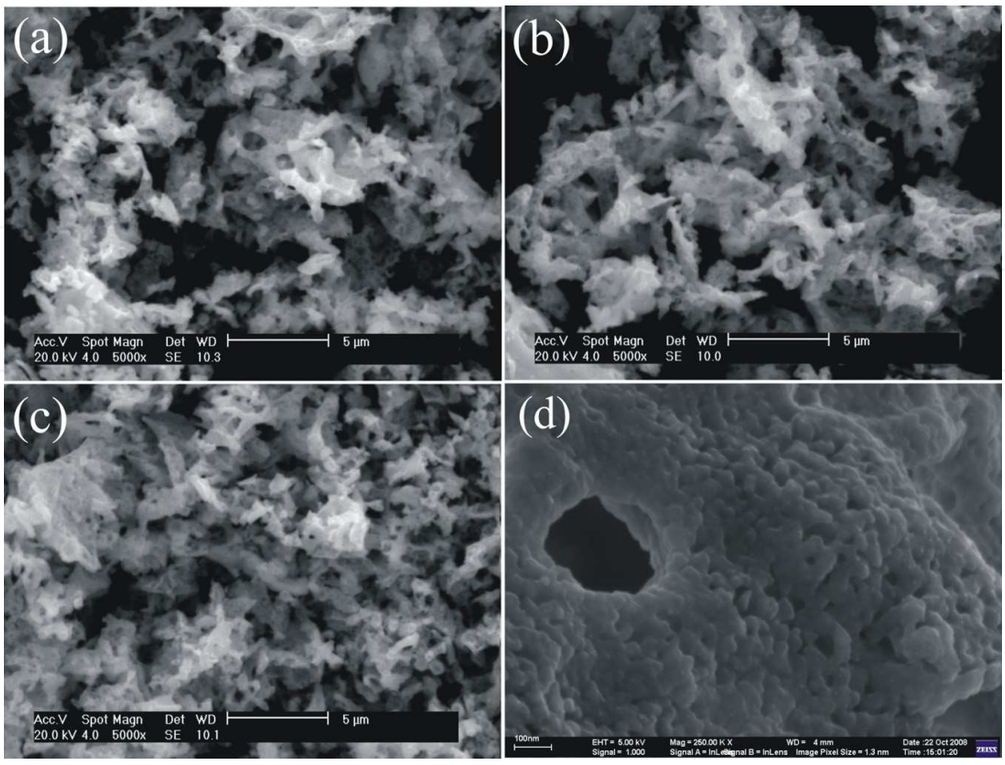

Fig. 4. SEM micrographs of LSM powders calcined at: (a) 500 ºC, (b) 700 ºC and (c) 900 ºC for 4 h. FEG-SEM high magnification image of powder calcined at 900 °C (d).

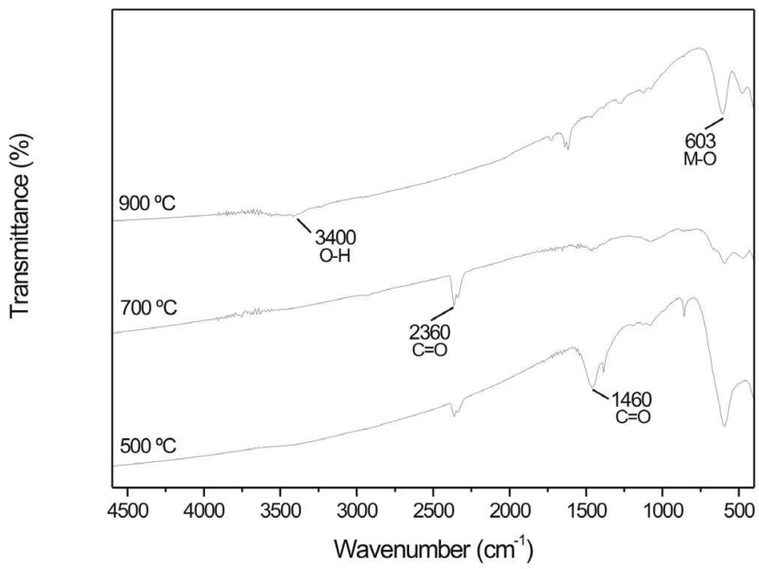

Fig. 5. FTIR spectra of LSM powders calcined at different temperatures.

The infrared reflectance spectrum in the FAR and MID ranges is presented in Fig. 6. The almost continuous decrease of the reflectivity as a function of the wave number shows that this spectrum is dominated by a conduction mechanism (Gosnet et al., 2008). Moreover, first

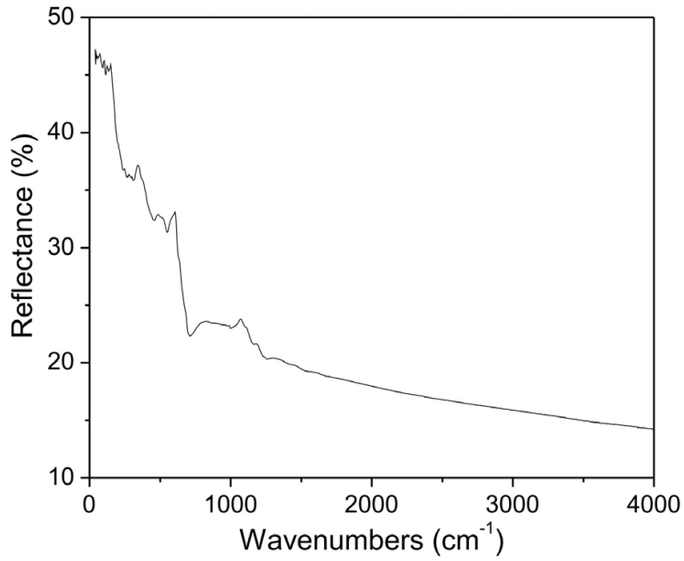

Fig. 6. Infrared reflectance spectrum in the FAR and MID ranges for LSM powder calcined at 900 °C.

order phonon features characteristic of the crystal lattice are clearly superposed on the decreasing reflectivity curve below 700 cm^{-1}. The reflectivity line shape of these phonons is rather characteristic of conducting materials and denotes possibly electron-phonon coupling in the LSM powder calcined at 900 °C, as also observed in $La_{0.7}Ca_{0.3}MnO_3$ ceramics (Kim et al., 1996). On the other hand, the two modes above 1000 cm^{-1} are likely to be defect modes from impurities due to unreacted materials, probably Mn_3O_4, as observed by XRD.

The XRD patterns of SDC powders, as synthesized by the modified Pechini method and after calcination from 700 to 900 °C, are shown in Fig. 7. XRD results revealed no peaks corresponding to secondary phases, i.e., there are no obvious peaks from phases other than SDC (JCPDS 75-0158) until the detection limit of the X-ray diffraction. The Rietveld refinement of the diffraction data using Maud program indicates that SDC powders exhibit cubic structures with space group Fm-3m and crystallite sizes in the range of 7-38 nm. Typical particle morphology of the SDC powder calcined at 900 °C is shown in Fig. 7(b), from which it can be seen that the particles are nearly spherical and strongly agglomerated, as expected for nanoparticles synthesized by the polymeric precursor method. FEG-SEM images also showed that the spherical particles are lower than 50 nm.

The FTIR spectra of SDC powders synthesized by the modified Pechini method and calcined at different temperatures are shown in Fig. 8. The peaks at around 3400 and 1640 cm^{-1} correspond to the H-O stretching and H-O-H bending vibration, respectively. They indicate that water or hydroxyl groups still existed not only in the as-prepared, but also in all calcined samples. A low intensity band at 1380 cm^{-1} in the as-prepared powder might indicate the physical adsorption of CO_2 or be caused by residual NO^{3-} (Chen et al., 2006). However, this band is eliminated after heat treatment. Therefore, although a synthesis temperature as low as 350 °C was sufficient to produce the SDC phase, powders with higher purity were obtained by calcining above 700 °C.

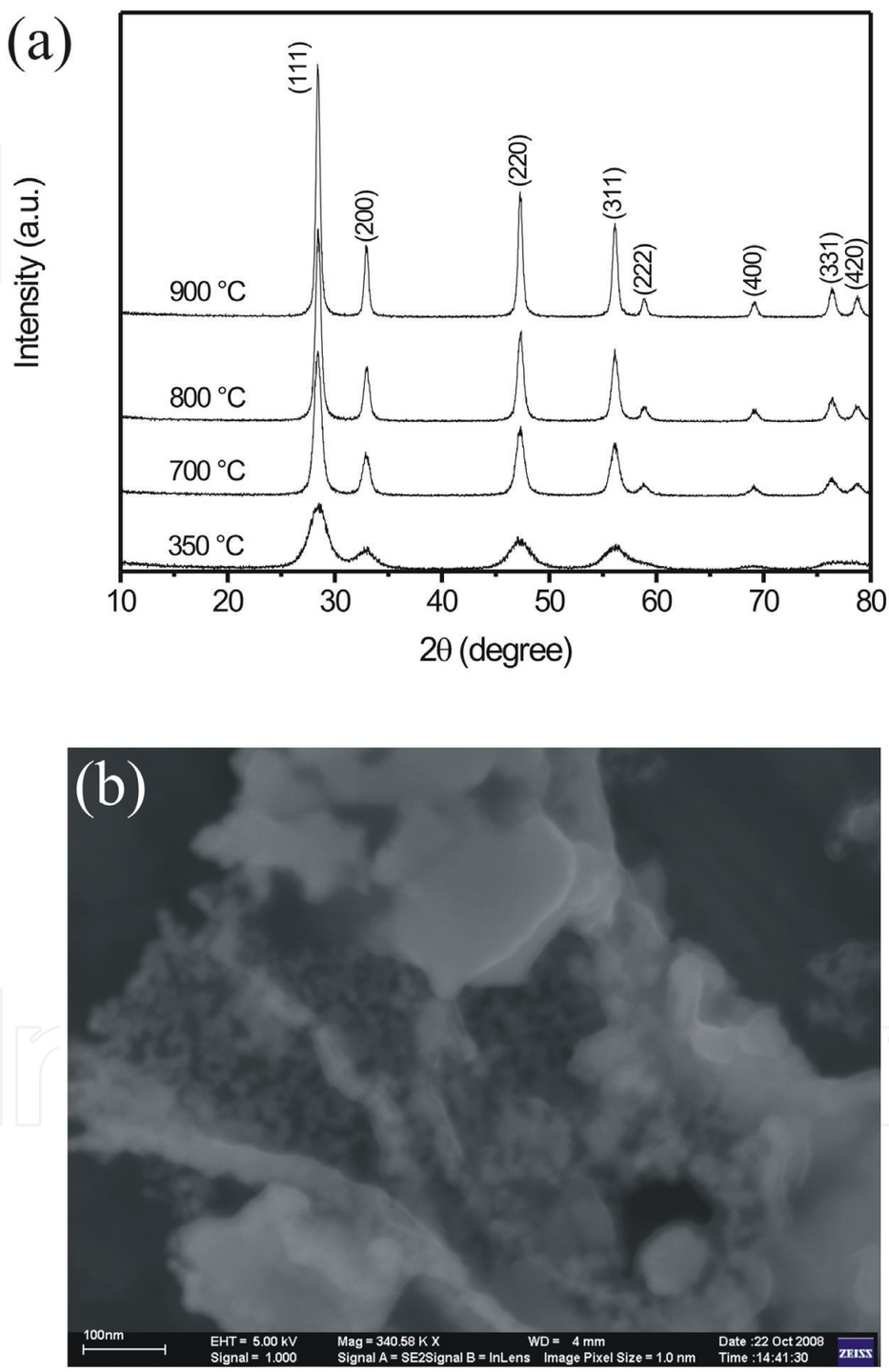

Fig. 7. XRD patterns of SDC powders calcined at different temperatures (a) and FEG-SEM image of the SDC powder calcined at 900 °C (b).

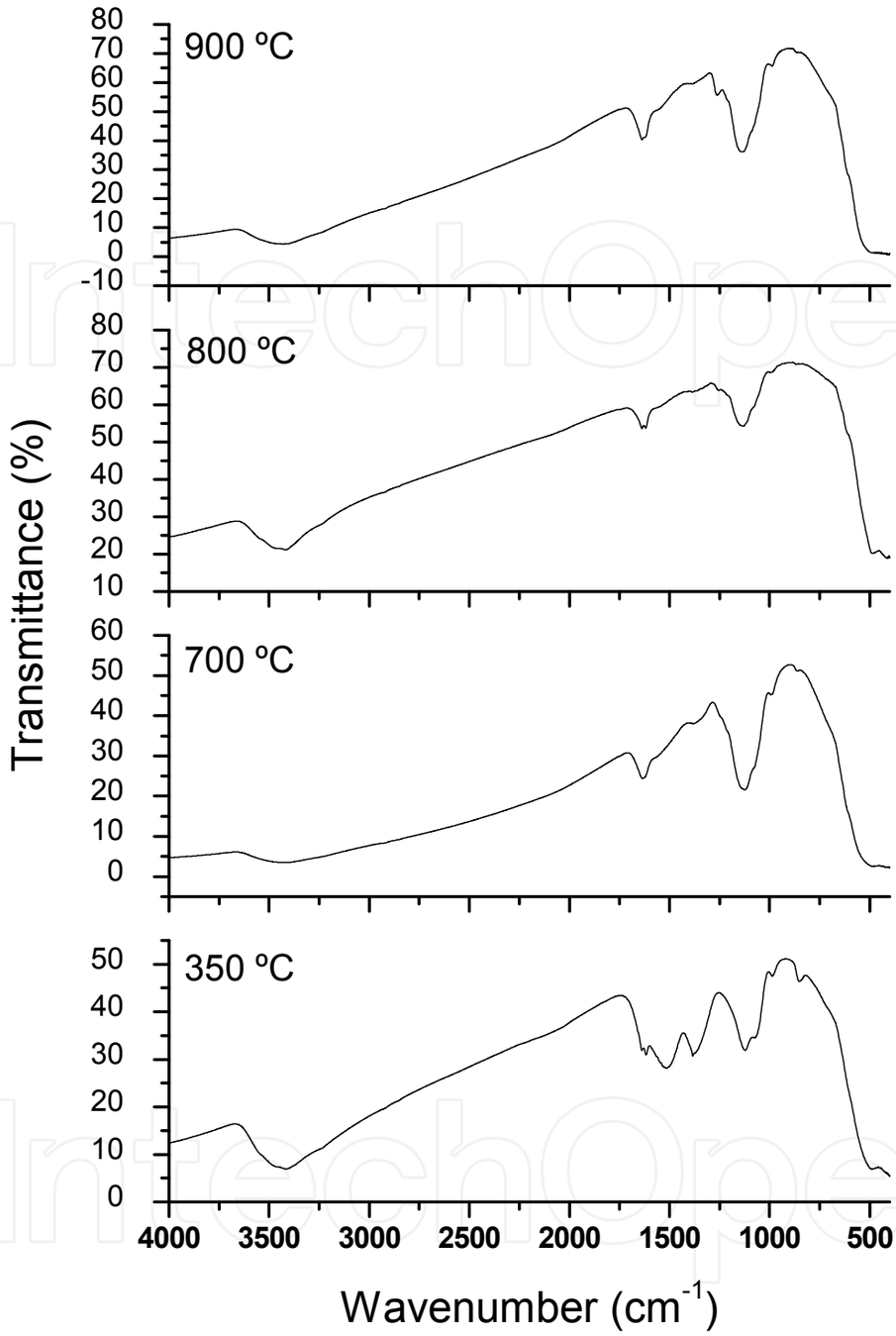

Fig. 8. FTIR spectra of SDC powders at different temperatures.

Fig. 9 shows the XRD patterns of LSCF powder both as-prepared and calcined at 900 °C for 4 h. Prior to calcination and after only 1 minute of microwave irradiation, the powder already exhibited mainly the perovskite-type structure. In addition, some peaks of deleterious phases ($LaCoO_4$ and $SrCO_3$) were detected before calcination. The formation of $SrCO_3$ can be attributed to the reaction of $Sr(NO_3)_2$ and CO_2. Compared with the as-prepared powder, the LSCF powder after calcination displayed higher crystallization. Since carbonaceous phases

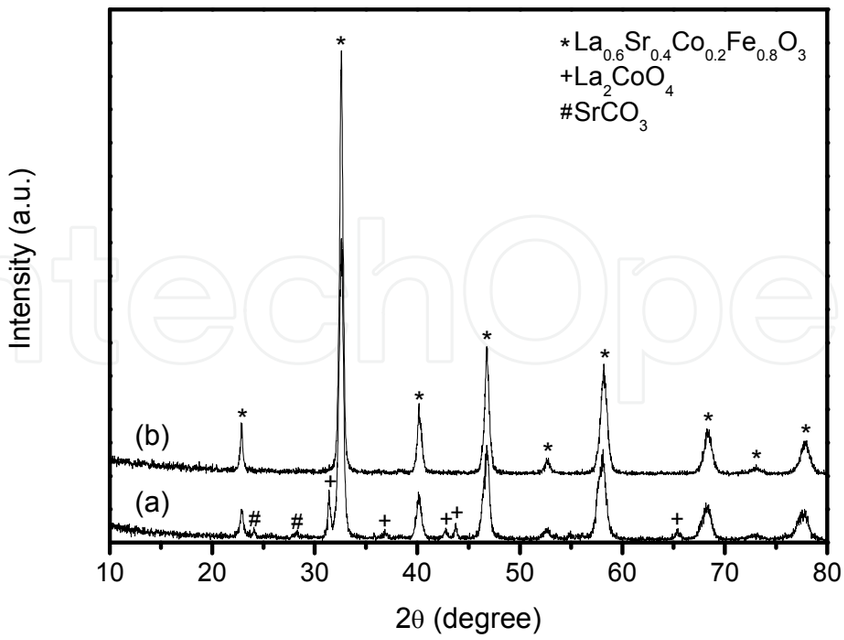

Fig. 9. XRD patterns of LSCF powder: (a) as-prepared and (b) calcined at 900 °C.

may dramatically deteriorate the cathode performance for SOFCs due to its poisoning effect on the cathode surface, further calcination at 900 °C under air for 4 h was carried out in order to eliminate the $SrCO_3$ impurity, driving its decomposition to CO_2. Accompanied by the formation of $SrCO_3$, another K_2NiF_4-structured phase with many small peaks was identified in the as-prepared LSCF powder. This phase was ascribed as La_2CoO_4, based on JCPDS card 34–1296. It is important to mention that it has good electronic and oxygen ionic conductivity and activity for oxygen reduction, being therefore, expected to have negligible effect on the cathode performance of LSCF (Borovskikh et al., 2003; Vashook et al., 2000). In any case, it is observed that both secondary phases decomposed completely after calcination.

Fig. 10 shows SEM images of the LSCF powder after calcination at 900 °C. As expected for ceramic materials synthesized by the combustion method, the powder presents a porous microstructure consisting of small uniform particles. The porous structure of this material can be attributed to significant gas evolution during the combustion reaction.

Fig. 11 shows the FTIR spectra for the as-prepared and calcined LSCF powders. The strong absorption bands in the low wave number region (~ 595 cm^{-1}) are associated with metal-oxygen (M-O) bonds characteristic of the perovskite structure. The similar absorption intensity of this band confirms that the perovskite-type structure is almost completely obtained after the combustion reaction, as observed by X-ray diffraction. The band at 1620 cm^{-1} corresponds to the stretching vibration frequency of coordinated H_2O (δ_{HOH}). The bands related to absorbed water (3400 cm^{-1}) were also present in both samples. Before calcination at 900 °C for 4 h, the LSCF powder exhibited strong absorption bands at 1381 cm^{-1} and 1454 cm^{-1}, which indicate the characteristic vibration of NO_3^{-1} and the stretching of the CO_3^{2-}, respectively. Based on these results, it is possible to conclude that during LSCF synthesis, some nitrates can react with carbon dioxide to form carbonaceous phases which decompose after further calcination at 900 °C for 4 h. Therefore, FTIR results are consistent with XRD analyses.

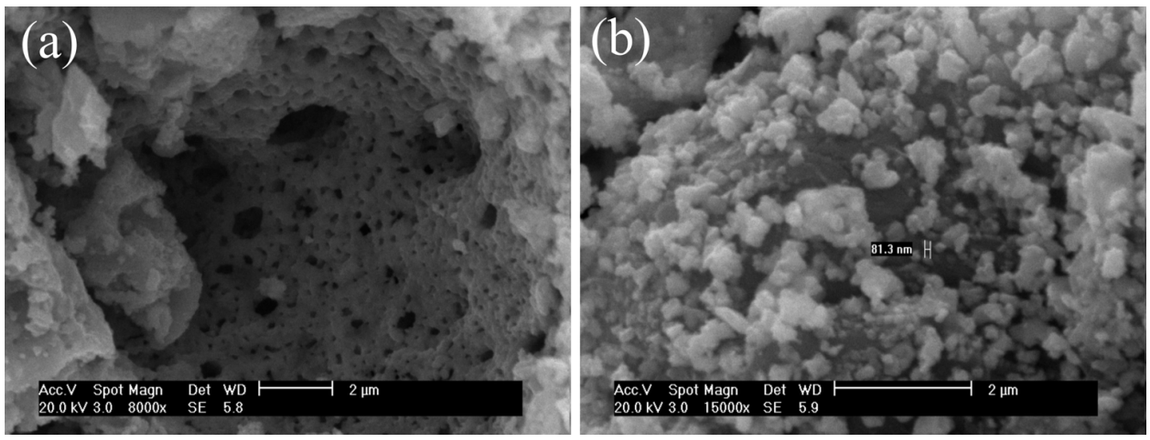

Fig. 10. SEM images of LSCF powder calcined at 900 °C: (a) porous structure and (b) typical small particles.

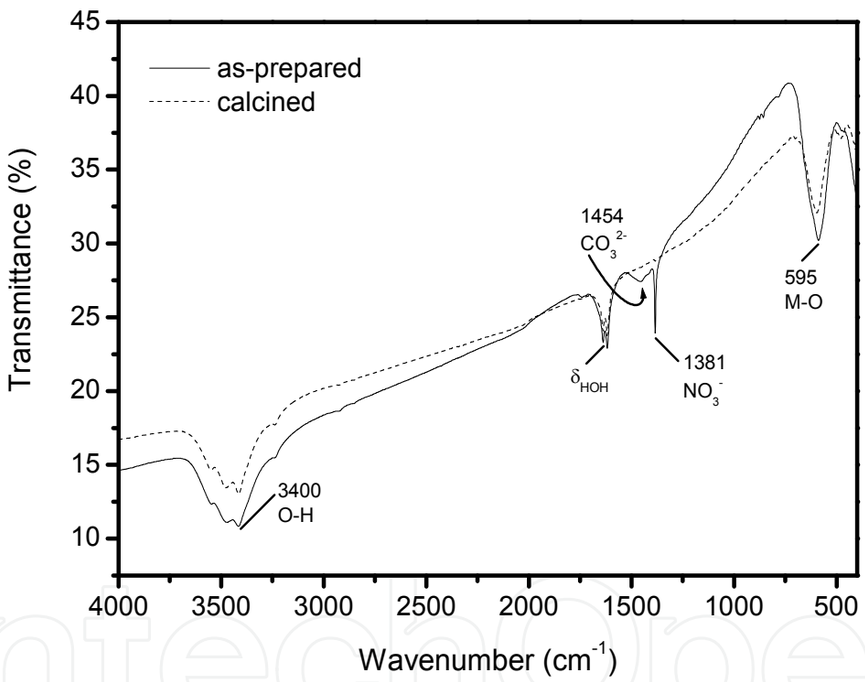

Fig. 11. FTIR spectra for the as-prepared and calcined LSCF powders.

5.1.1 Characterization of composite cathodes

LSM, SDC and LSCF powders synthesized by the above mentioned methods were used to prepare LSM-SDC and LSCF-SDC composite films onto YSZ substrates. A previous study performed by Ye and co-workers (Ye et al., 2007) demonstrated that the amount of ethyl cellulose in LSM-SDC slurries is restricted by cracking of the surface of the films. These authors observed that cracking took place when the amount of pore former reached 15 wt.% and is caused by the large amount of organics which evaporates during sintering. Therefore, in the present study, LSM-SDC slurries with a maximum of 10 wt.% ethyl cellulose were used. Fig. 12 shows FEG-SEM images of the porous structure of LSM-SDC composite

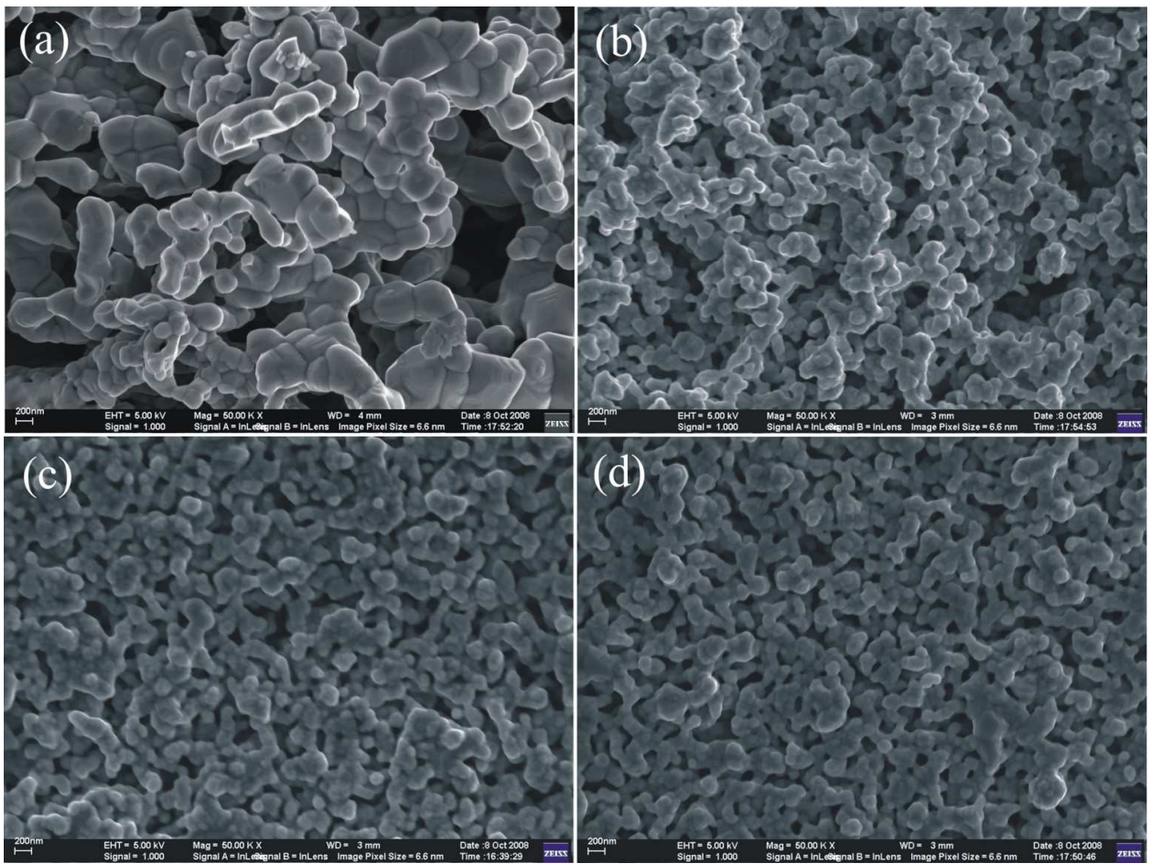

Fig. 12. FEG-SEM images of the surface of LSM-SDC composite cathodes containing different amounts of ethyl cellulose: (a) 0 wt.%, (b) 4 wt.%, (c) 8 wt.%, (d) 10 wt.%.

cathodes containing different amounts of ethyl cellulose. In these images, it is possible to observe the effects of the milling process and the addition of ethyl cellulose in the final microstructure of composite cathodes. The film obtained without addition of ethyl cellulose and without prior milling treatment of powders (Fig. 12a) depicted particle sizes of about 200 nm. On the other hand, in the films obtained with the powders previously milled for 24 h (Figure 12b-d) it can be observed that both particle agglomeration and pore size decrease as the ethyl cellulose content increases. Moreover, the particle size is lower than 200 nm. Typically, if the slurry contains 10 wt.% ethyl cellulose (Fig. 12d), the film exhibits a highly porous surface morphology and uniform pore structure, which are essential conditions for obtaining high-performance cathodes. The electrochemical evaluation of these composite cathodes are currently under way.

Fig. 13 shows cross-sectional SEM images of the LSM-SDC cathodes containing 0 and 10 wt.% ethyl cellulose after milling LSM and SDC powders. The film without addition of ethyl cellulose (Fig. 13a) is tightly adhered to the substrate and shows few pores. However, the film containing 10 wt.% ethyl cellulose (~ 10 µm thick) is also well adhered to the YSZ substrate and exhibits higher pore uniformity than that in Fig. 13a. Such a porous microstructure fulfils the need for a SOFC cathode, which possess high active surface area, while permitting rapid diffusion of oxygen through the porous cathode film.

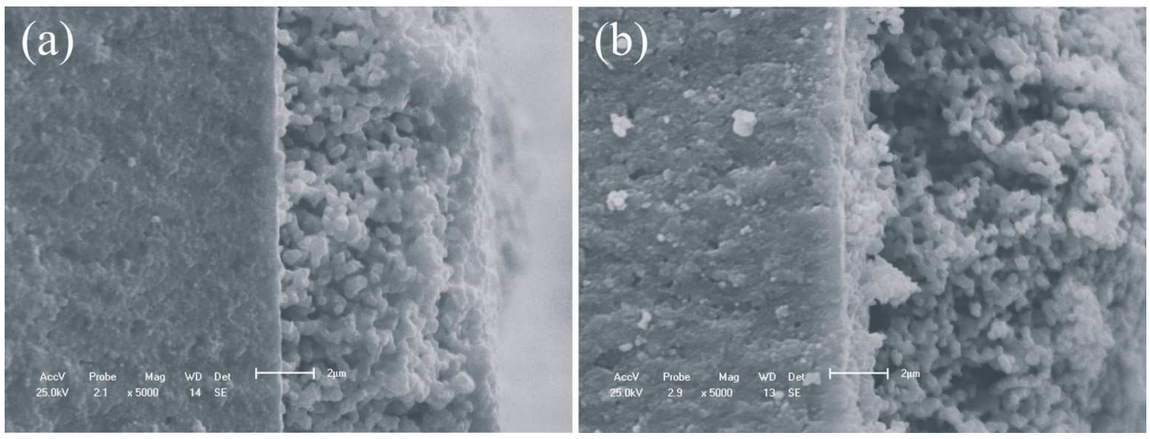

Fig. 13. Cross-sectional SEM images of LSM-SDC cathodes containing different amounts of ethyl cellulose: (a) 0 wt.% and (b) 10 wt.%.

5.2 Characterization of a SOFC single cell

A SEM micrograph of the cathode/electrolyte interface and preliminary results on the electrochemical activity of YSZ electrolyte-supported SOFCs containing Ni-YSZ anode and a LSCF-SDC composite cathode are shown in Fig. 14. As it can be seen in Fig. 14(a), the composite film not only has good adhesion to the electrolyte, but also possesses a porous microstructure which is required for the oxidant electrochemical reduction. It indicates that such a composite film can have a good performance as SOFC cathode. By the LSV technique, qualitative information about electrochemical activity of this SOFC was acquired. The power density curves (Fig. 14b) revealed that maximum power densities were 19, 26, 36 and 46 mW/cm^2 at 800, 850, 900 and 950 ^{o}C. It is possible to compare these first results with literature data and safely state that the LSCF-SDC cathode composite is qualitatively better than other plain standard materials or cathode composites already reported. It should also be mentioned that the result obtained at 800 ^{o}C is similar to that reported by Muccillo et al (Muccillo et al., 2006) for a SOFC single cell with LSM-YSZ cathode, Ni-YSZ anode and 70 µm

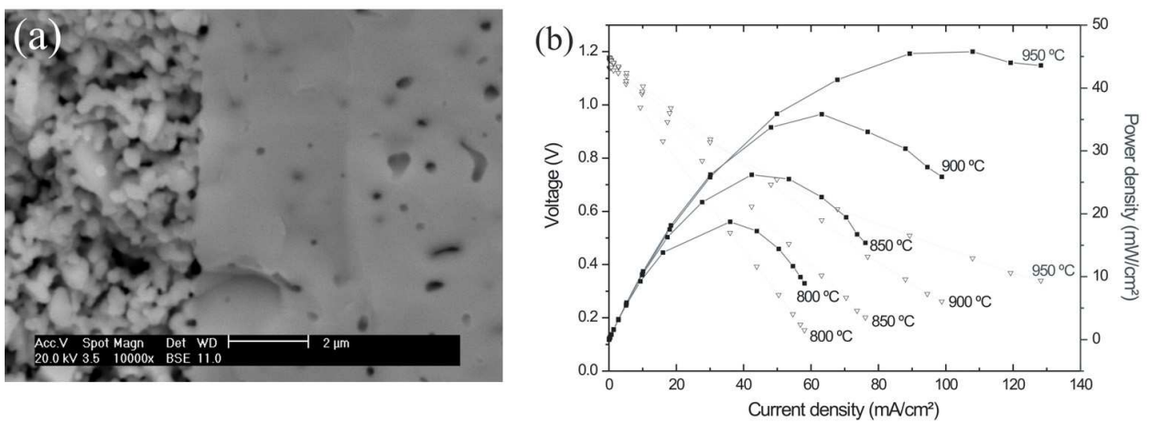

Fig. 14. Electrolyte-supported SOFC: (a) SEM micrograph of the cathode (LSCF-SDC)/electrolyte (YSZ) interface, (b) I-V and power density curves at different temperatures.

thick YSZ electrolyte. Nonetheless, voltage and power density values cannot be compared to literature data because of the thick (200 μm) electrolyte used as cell support, which is responsible for high ohmic polarization. The improvement in cell performance is attributed to the good catalytic activity of the novel LSCF-SDC composite film prepared from the powders obtained by different synthesis methods.

6. Conclusions

Results showed that LSM, SDC and LSCF powders were successfully synthesized by modified Pechini and microwave-assisted combustion methods. The milling process of the LSM-SDC composite powders and the addition of ethyl cellulose to the slurries seem to reduce particle agglomeration and pore size, that could improve the triple phase boundary (TPB) and, consequently, the electrochemical efficiency of the cathode. According to the results gathered herein, LSM-SDC films containing 10 wt.% ethyl cellulose (maximum concentration in order to avoid surface cracks) exhibited uniform and continuous pore structure and excellent adhesion to the YSZ substrate. The composite films produced presented porous microstructures desirable for the electrochemical reduction of the oxidant. Homogeneity and agglomeration absence or phase segregation were also characteristics found in the composite films prepared.

FTIR technique was successfully applied for powder characterization. Results were in agreement with XRD data, demonstrating that the FTIR is also a powerful tool for evaluating the crystalline structure evolution after a chemical synthesis. Moreover, the data could also indicate that water or hydroxyl groups still existed for some calcinated samples as well as physical adsorption of CO_2, giving a qualitative information of purity of the samples.

7. Acknowledgments

The authors acknowledge PPGCEM-UFRN, PPGQ-UFRN, PRH-ANP 14, CAPES (PRÓ-ENGENHARIAS and PDEE program – BEX 6775/10-1), CAPES-PROCAD, and CNPq (477294/2006-5, 502238/2007-0 and 554576/2010-4) for their financial support.

8. References

Atkinson, A.; Barnett, S.; Gorte, R. J.; Irvine, J. T. S.; McEvoy, A. J.; Mogensen, M.; Singhal, S. C.; Vohs J. (2004). Advanced anodes for high-temperature fuel cells. *Nature Materials*, Vol. 3, pp. (17-27), ISSN 1476-1122

Borovskikh, L.; Mazo, G.; Kemnitz, E. (2003). Reactivity of oxygen of complex cobaltates $La_{1-x}Sr_xCoO_{3-\delta}$ and $LaSrCoO_4$. *Solid State Sciences*, Vol. 5, No. 3, (23 March 2003), pp. (409–17), ISSN 1293-2558

Cela, B.; Macedo, D. A.; Souza, G. L.; Nascimento, R. M.; Martinelli, A. E.; Paskocimas, C. A. (2009). Strontium-doped lanthanum manganite synthesis for solid oxide fuel cells cathode. *Journal of New Materials for Electrochemical Systems*, Vol. 12, No. 2-3, (1 April 2009), pp. (109-113), ISSN 1480-2422

Chen, K.; Lü, Z.; Ai, N.; Chen, X.; Hu, J.; Huang, X.; Su, W. (2007). Effect of SDC-impregnated LSM cathodes on the performance of anode-supported YSZ films for SOFCs. *Journal of Power Sources*, Vol. 167, No. 1, (1 May 2007), pp. (84-89), ISSN 0378-7753

Chen, M.; Kim, B. H.; Xu, Q.; Nam, O. J.; Ko, J. H. (2008). Synthesis and performances of Ni–SDC cermets for IT-SOFC anode. *Journal of the European Ceramic Society,* Vol. 28, No 15, (November 2008), pp. (2947-2953), ISSN 0955-2219

Chen, W.; Li, F.; Yu, J. (2006). Combustion synthesis and characterization of nanocrystalline CeO_2-based powders via ethylene glycol–nitrate process. *Material Letters*, Vol. 60, No. 1, (January 2006), pp. (57–62), ISSN 167-577X

Conceição, L.; Silva, A. M.; Ribeiro, N. F. P.; Souza, M. M. V. M. (2011). Combustion synthesis of $La_{0.7}Sr_{0.3}Co_{0.5}Fe_{0.5}O_3$ (LSCF) porous materials for application as cathode in IT-SOFC. *Materials Research Bulletin*, Vol. 46, No. 2, (February 2011), pp. (308-314), ISSN 0025-5408

Conceição, L.; Silva, R. C. B.; Ribeiro, N. F. P.; Souza, M. M. V. M. (2009). Influence of the synthesis method on the porosity, microstructure and electrical properties of $La_{0.7}Sr_{0.3}MnO_3$ cathode materials. *Materials Characterization,* Vol. 60, No. 12, (December 2009), pp. (1417-1423), ISSN 1044-5803

Escobedo, C. A. C.; Saldaña, J. M.; Miró, A. M. B.; Jesús, F. S. (2008). Determination of strontium and lanthanum zirconates in YPSZ–LSM mixtures for SOFC. *Journal of Power Sources*, Vol. 180, No. 1, (15 May 2008), pp. (209-214), ISSN 0378-7753

Gosnet, A. M. H.; Koubaa, M.; Santander-Syro, A. F.; Lobo, R. P. S. M.; Lecoeur, P.; Mercey, B. (2008). Metallic nature of strained thin single-crystal $La_{2/3}Sr_{1/3}MnO_3$ films. *Physical Review B*, Vol. 78, No. 11, (September 2008), Article Number 115118, pp. (1-5), ISSN 1098-0121

Grossin, D.; Noudem, J. G. (2004). Synthesis of fine $La_{0.8}Sr_{0.2}MnO_3$ powder by different ways. *Solid State Sciences*, Vol. 6, No. 9, (September 2004), pp. 939-944, ISSN 1293-2558

Guo, H.; Iqbal, G.; Kang, B. S. (2010). Development of an In Situ Surface Deformation and Temperature Measurement Technique for a Solid Oxide Fuel Cell Button Cell. *International Journal of Applied Ceramic Technology*, Vol. 7, No. 1, (January/February 2010), pp. (55-62), ISSN 1744-7402

Guo, R. S.; Wei, Q. T.; Li, H. L.; Wang, F. H. (2006). Synthesis and properties of $La_{0.7}Sr_{0.3}MnO_3$ cathode by gel combustion. *Materials Letters*, Vol. 60, No. 2, (January 2006), pp. 261-265, ISSN 0167-577X

Ivers-Tiffee, E.; Weber, A.; Herbstritt, D. (2001). Materials and technologies for SOFC-components. *Journal of the European Ceramic Society*, Vol. 21, No. 10-11, (22 August 2001), pp. (1805-1811), ISSN 0955-2219

Jiang, S. P. (2003). Issues on development of (La,Sr)MnO_3 cathode for solid oxide fuel cells. *Journal of Power Sources,* Vol. 124, No. 2, (24 November 2003), pp. (390-402), ISSN 0378-7753

Kim, K. H.; Gu, J. Y.; Choi, H. S.; Park, J. W.; Noh, T. W. (1996), Frequency Shifts of the Internal Phonon Modes in $La_{0.7}Ca_{0.3}MnO_3$. *Physical Review Letters*, Vol. 77, No. 9, (26 August 1996), pp. (1877 – 1880), ISSN 0031-9007

Konysheva, E.; Irvine, J. T. S.; Besmehn, A. (2009). Crystal structure, thermochemical stability, electrical and magnetic properties of the two-phase composites in the $La_{0.8}Sr_{0.2}MnO_{3\pm\delta}$–$CeO_2$ system. *Solid State Ionics*, Vol. 180, No. 11-13, (22 June 2009), pp. (778-783), ISSN 0167-2738

Lin, H.; Ding, C.; Sato, K.; Tsutai, Y.; Ohtaki, H.; Iguchi, M.; Wada, C.; Hashida, T. (2008). Preparation of SDC electrolyte thin films on dense and porous substrates by modified sol–gel route. *Materials Sciences and Engineering B*, Vol. 148, No. 1-3, (25 February 2008), pp. (73-76), ISSN 0921-5107

Liu, S.; Qian, X.; Xiao. (2007). Synthesis and characterization of $La_{0.8}Sr_{0.2}Co_{0.5}Fe_{0.5}O_{3\pm\delta}$ nanopowders by microwave assisted sol–gel route, *Journal of Sol-Gel Science and Technology*, Vol. 44, No. 3, (3 October 2007), pp. (187-193), ISSN 0928-0707

Liu, X.; Faguy, P. W.; Liu, M. (2002). In Situ Potential-Dependent FTIR Emission Spectroscopy. *Journal of The Electrochemical Society*, Vol. 149, No. 10, 2002, pp. (1293-1298), ISSN 1945-7111 (online)

Macedo, D. A.; Cela, B.; Martinelli, A. E.; Nascimento, R. M.; Melo, D. M. A.; Paskocimas, C. A.; Rabelo, A. A. (2009) Synthesis, processing and characterization of ZrO_2-$8Y_2O_3$, ZrO_2-$8CeO_2$ and $La_{0.78}Sr_{0.22}MnO_3$ powders. *Journal of New Materials for Electrochemical Systems*, Vol. 12, No. 2-3, (1 April 2009), pp. (103-108), ISSN 1480-2422

Maia, A. O. G.; Meneses, C. T.; Menezes, A. S.; Flores, W. H.; Melo, D. M. A.; Sasaki, J. M. (2006). Synthesis and X-ray structural characterization of NiO nanoparticles obtained through gelatin. *Journal of Non-Crystalline Solids*, Vol. 352, No. 32-35, (15 September 2006), pp. (3729-3733), ISSN 0022-3093

McIntosh S.; Gorte R. J. (2004). Direct Hydrocarbon Solid Oxide Fuel Cells. *Chemical Reviews*, Vol. 104, No. 10, (21 July 2004), pp. (4845-4866), ISSN 0009-2665

Medeiros, A. M. L.; Miranda, M. A. R.; Menezes, A. S.; Jardim, P. M.; Silva, L. R. D.; Gouveia, S. T.; Sasaki, J. M. (2004). Synthesis and Characterization of Cr_2O_3 Nanoparticles Obtained by Gelatin. *Journal of Metastable and Nanocrystalline Materials*, Vol. 20-21, pp. (399-406), ISSN 1422-6375

Minh, N. Q. & Takahashi T (1995). Science and Technology of Ceramic Fuel Cell, Elsevier Science, ISBN 0-444-89568-X, Amsterdam, The Netherlands.

Minh, N. Q. (1993). Ceramic fuel cells. *Journal of the American Ceramic Society*, Vol. 76, No. 563, (March 1993), pp. (563–588), ISSN 1551-2916

Minh, N. Q. (2004). Solid oxide fuel cell technology—features and applications. *Solid State Ionics*, Vol. 174, No. 1-4, (29 October 2004), pp. (271-277), ISSN 0167-2738

Molenda, J.; Swierczek, K.; Zajac, W. (2007). Functional materials for the IT-SOFC. *Journal of Power Sources*, Vol. 173, No. 2, (15 November 2007), pp. (657-670), ISSN 0378-7753

Muccillo, R.; Muccillo, E. N. S.; Fonseca, F. C.; França, Y. V.; Porfírio, T. C.; Florio, D. Z.; Berton, M. A. C.; Garcia, M. C. (2006). Development and testing of anode-supported solid oxide fuel cells with slurry-coated electrolyte and cathode. *Journal of Power Sources*, Vol. 156, No. 2, (1 June 2006), pp. (455-460), ISSN 0378-7753

Pechini, M. P. (1967). Method of preparing lead and alkaline earth titanates and niobates and coating method using the same to form a capacitor. US Patent No. 3,330,697 (11 July 1967)

Resini, C.; Venkov, T.; Hadjiivanov, K.; Presto S.; Riani, P.; Marazza, R.; Ramis, G.; Busca, G. (2009). An FTIR study of the dispersed Ni species on Ni-YSZ catalysts. *Applied Catalysis A: General,* Vol. 353, No. 1, (January 2009), pp. (137-143), ISSN 0926-860X

Shao, J.; Tao, Y.; Wang, J.; Xu, C.; Wang, W. G. (2009). Investigation of precursors in the preparation of nanostructured $La_{0.6}Sr_{0.4}Co_{0.2}Fe_{0.8}O_{3-\delta}$ via a modified combined complexing method. *Journal of Alloys and Compounds,* Vol. 484, No. 1-2, (18 September 2009), pp. (263-267), ISSN 0925-8388

Singhal, S. C. (2000). Advances in solid oxide fuel cell technology. *Solid State Ionics*, Vol. 135, No. 1-4, (1 November 2000), pp. (305-313), ISSN 0167-2738

Steele B. C. H.; Heinzel, A. (2001). Materials for fuel-cell technologies. *Nature*, Vol. 414, (15 November 2001), pp. (345-352), ISSN 0028-0836

Steele, B. C. H. (2000). Appraisal of $Ce_{1-y}Gd_yO_{2-y/2}$ electrolytes for IT-SOFC operation at 500°C. *Solid State Ionics*, Vol. 129, No. 1-4, (April 2000), pp. (95-110), ISSN 0167-2738

Stuart, B. H (2004). Infrared Spectroscopy: Fundamentals and Applications (Analytical Techniques in the Sciences (AnTs) *), John Wiley and Son's Ltd. England.

Tsai, T.; Barnett, S. A. (1997). Effect of LSM-YSZ cathode on thin-electrolyte solid oxide fuel cell performance. *Solid State Ionics*, Vol. 93, No. 3-4, (January 1997), pp. (207-217), ISSN 0167-2738

Vargas, R. A.; Chiba, R. ; Andreoli, M.; Seo, E. S. M. (2008). Synthesis and characterization of $La_{1-x}Sr_xMnO_{3\pm\delta}$ and $La_{1-x}Sr_xCo_{1-y}Fe_yO_{3-\delta}$ used as cathode in solid oxide fuel cells. *Cerâmica*, Vol. 54, No. 331, (July - September 2008), pp. (366-372), ISSN 0366-6913

Vashook, V. V.; Ullmann, H.; Olshevskaya, O. P.; Kulik, V. P.; Lukashevich, V. E.; Kokhanovskij, L. V. (2000). Composition and electrical conductivity of some cobaltates of the type $La_{2-x}Sr_xCoO_{4.5-x/2\pm\delta}$. *Solid State Ionics*, Vol. 138, No. 1-2, (4 December 2000), pp. (99–104), ISSN 0167-2738

Wang, K.; Ran, R.; Shao, Z. (2007). Methane-fueled IT-SOFCs with facile in situ inorganic templating synthesized mesoporous $Sm_{0.2}Ce_{0.8}O_{1.9}$ as catalytic layer. *Journal of Power Sources*, Vol. 170, No. 2, (10 July 2007), pp. (251-258), ISSN 0378-7753

Xu, X.; Cao, C.; Xia, C.; Peng, D. (2009). Electrochemical performance of LSM–SDC electrodes prepared with ion-impregnated LSM. *Ceramics International*, Vol. 35, No. 6, (August 2009), pp. (2213-2218), ISSN 0272-8842

Xu, X.; Jiang, Z.; Fan, X.; Xia, C. (2006). LSM–SDC electrodes fabricated with an ion-impregnating process for SOFCs with doped ceria electrolytes. *Solid State Ionics*, Vol. 177, No. 19-25, (15 October 2006), pp. (2113-2117), ISSN 0167-2738

Xu, X.; Xia, C.; Xiao, G.; Peng, D. (2005). Fabrication and performance of functionally graded cathodes for IT-SOFCs based on doped ceria electrolytes. *Solid State Ionics*, Vol. 176, No. 17-18, (31 May 2005), pp. (1513-1520), ISSN 0167-2738

Yang, K.; Shen, J. H.; Yang, K. Y.; Hung, I. M.; Fung, K. Z.; Wang, M. C. (2007). Characterization of the yttria-stabilized zirconia thin film electrophoretic deposited on $La_{0.8}Sr_{0.2}MnO_3$ substrate. *Journal of Alloys and Compounds,* Vol. 436, No. 1-2, (14 June 2007), pp. (351-357), ISSN 0925-8388

Ye, F., Wang, Z.; Weng W.; Cheng, K.; Song, C.; Du, P.; Sheng, G.; Han, G. (2007). Spin-coating derived LSM-SDC films with uniform pore structure. *Thin Solid Films*, Vol. 516, No. 16, (30 June 2008), pp. (5206-5209), ISSN 0040-6090

Zhang, L.; Zhao, F.; Peng, R.; Xia, C. (2008). Effect of firing temperature on the performance of LSM–SDC cathodes prepared with an ion-impregnation method. *Solid State Ionics*, Vol. 179, No. 27-32, (30 September 2008), pp. (1553-1556), ISSN 0167-2738

Zhang, Y.; Huang, X.; Lu, Z.; Liu, Z.; Ge, X.; Xu, J.; Xin, X.; Sha, X.; Su, X. (2007). Ni–$Sm_{0.2}Ce_{0.8}O_{1.9}$ anode-supported YSZ electrolyte film and its application in solid oxide fuel cells. *Journal of Alloys and Compounds*, Vol. 428, No. 1-2, (31 January 2007), pp. (302-306), ISSN 0925-8388

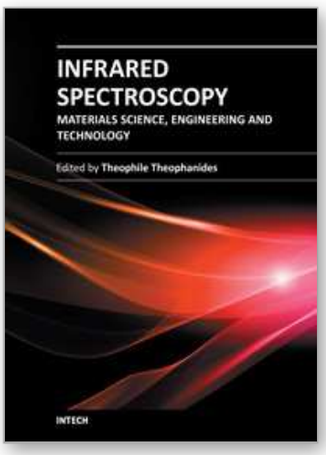

Infrared Spectroscopy - Materials Science, Engineering and Technology

Edited by Prof. Theophanides Theophile

ISBN 978-953-51-0537-4
Hard cover, 510 pages
Publisher InTech
Published online 25, April, 2012
Published in print edition April, 2012

The present book is a definitive review in the field of Infrared (IR) and Near Infrared (NIR) Spectroscopies, which are powerful, non invasive imaging techniques. This book brings together multidisciplinary chapters written by leading authorities in the area. The book provides a thorough overview of progress in the field of applications of IR and NIR spectroscopy in Materials Science, Engineering and Technology. Through a presentation of diverse applications, this book aims at bridging various disciplines and provides a platform for collaborations among scientists.

How to reference

In order to correctly reference this scholarly work, feel free to copy and paste the following:

Daniel A. Macedo, Moisés R. Cesário, Graziele L. Souza, Beatriz Cela, Carlos A. Paskocimas, Antonio E. Martinelli, Dulce M. A. Melo and Rubens M. Nascimento (2012). Infrared Spectroscopy Techniques in the Characterization of SOFC Functional Ceramics, Infrared Spectroscopy - Materials Science, Engineering and Technology, Prof. Theophanides Theophile (Ed.), ISBN: 978-953-51-0537-4, InTech, Available from: http://www.intechopen.com/books/infrared-spectroscopy-materials-science-engineering-and-technology/infrared-spectroscopy-techniques-in-the-characterization-of-sofc-functional-ceramics

INTECH
open science | open minds

InTech Europe
University Campus STeP Ri
Slavka Krautzeka 83/A
51000 Rijeka, Croatia
Phone: +385 (51) 770 447
Fax: +385 (51) 686 166
www.intechopen.com

InTech China
Unit 405, Office Block, Hotel Equatorial Shanghai
No.65, Yan An Road (West), Shanghai, 200040, China
中国上海市延安西路65号上海国际贵都大饭店办公楼405单元
Phone: +86-21-62489820
Fax: +86-21-62489821

IntechOpen